

Fast Design Space Exploration of Nonlinear Systems: Part II

Prerit Terway^{ID}, Kenza Hamidouche^{ID}, and Niraj K. Jha^{ID}, *Fellow, IEEE*

Abstract—Nonlinear system design is often a multiobjective optimization problem involving the search for a design that satisfies a number of predefined constraints. The design space is typically very large since it includes all possible system architectures with different combinations of components composing each architecture. In this article, we address nonlinear system design space exploration through a two-step approach encapsulated in a framework called fast design space exploration of nonlinear systems (ASSENT). In the first step, we use a genetic algorithm to search for system architectures that allow discrete choices for component values or else only component values for a fixed architecture. This step yields a coarse design since the system may or may not meet the target specifications. In contrast to prior works on design space exploration that rely on forward design, we use an inverse design in step 2 to search over a continuous space and fine-tune the component values with the goal of improving the value of the objective function. We use a neural network (NN) to model the system response. The NN is converted into a mixed-integer linear program for active learning to sample component values efficiently. We illustrate the efficacy of ASSENT on problems ranging from nonlinear system design to the design of electrical circuits. Experimental results show that ASSENT achieves the same or better value of the objective function compared to various other optimization techniques for nonlinear system design by up to 53%. We improve sample efficiency by 6–12× compared to reinforcement learning-based synthesis of electrical circuits.

Index Terms—Active learning, evolutionary algorithm (EA), mixed-integer linear program (MILP), multiobjective optimization (MOO), neural networks (NNs), sample efficiency, system synthesis.

I. INTRODUCTION

NONLINEAR system design forms the core of various applications that include healthcare, smart grid, transportation, and smart home [1], [2]. The design of such systems involves solving a combinatorial optimization problem with a large design space of various system architectures and constituent components. It often requires solving a constrained multiobjective optimization (MOO) problem that arises in

several disciplines like circuit design and cyber-physical system synthesis. Typically, the designer has access to a black-box simulator but without knowledge of the underlying dynamics governing system response to inputs. To reduce the development time, the designer needs to minimize the number of calls to the simulator that may take anywhere from minutes to hours to even days to obtain the response for a given choice of input. Development time can be reduced through *active learning* of best inputs to simulate. The input sample can be selected based on past system response to inputs and the corresponding outputs.

Existing techniques for nonlinear system design include reinforcement learning (RL), Bayesian optimization (BO), and evolutionary algorithms (EAs) like genetic algorithm (GA). However, using RL and BO requires formulating MOO as a weighted sum of objectives. Setting the weights requires domain expertise and manual tuning. Moreover, deep RL requires access to a large number of graphical processing units (GPUs), thus increasing development cost. BO is generally very slow as the complexity of generating candidate solutions increases with an increase in the number of simulations. EAs like GA have been very successful in solving MOO problems. However, due to GA's inherent randomness, the algorithm needs to be executed over a large number of generations to meet system specifications. Thus, they are not sample-efficient. Surrogate-assisted EA can help improve the sample efficiency. The global search technique proposed in [3] uses the Gaussian process-based surrogate model and computes the probability of improvement to determine the candidate solution. This limits the methodology in [3] to a single objective or a weighted sum of objectives.

We propose ASSENT, a two-step methodology that builds upon CNMA¹ [4]: a sample-efficient exploration method that is described in detail in a sister Part I of this article. In contrast to CNMA that uses multiple solvers to escape local minima, in step 1 of ASSENT, we use GA to account for system response over the entire design space. CNMA determines component values for a fixed system architecture while ASSENT allows the exploration of system architecture and the component values or only the component values for a fixed architecture in step 1. We harness the benefits of GA to perform exploration in a discrete design space and the ease with which it can encode system architectures. We terminate GA after some stopping criteria are met even if the design requirements are not yet

Manuscript received 26 March 2021; revised 16 August 2021; accepted 23 September 2021. Date of publication 12 October 2021; date of current version 22 August 2022. This work was supported in part by the Defense Advanced Research Projects Agency (DARPA) and in part by the Air Force Research Laboratory (AFRL). This article was recommended by Associate Editor S. Mohanty. (*Corresponding author: Prerit Terway.*)

Prerit Terway and Niraj K. Jha are with the Department of Electrical Engineering, Princeton University, Princeton, NJ 08544 USA (e-mail: terway@princeton.edu; jha@princeton.edu).

Kenza Hamidouche is with the Department of Operations Research and Financial Engineering, Princeton University, Princeton, NJ 08544 USA (e-mail: kenzah@princeton.edu).

Digital Object Identifier 10.1109/TCAD.2021.3119274

¹CNMA stands for constrained optimization with NNs, MILP, and active learning.

met since GA is sample-inefficient and requires a large number of iterations to meet the requirements. We thus obtain a *coarse* design at the end of the first step.

In step 2, based on CNMA, we *fine-tune* the coarse design to search for component values in a continuous design space. This step uses a neural network (NN) as a surrogate function to model system response. We convert the NN into a mixed-integer linear program (MILP) to incorporate the constraints imposed by the permissible range of inputs (i.e., component values), outputs (i.e., desired response), and the MILP formulation of the NN. We use this formulation to obtain an *inverse design* of the system and find an input that satisfies the set of system constraints. A feasible solution of the MILP yields the input that is used to simulate the system. In the case of an infeasible solution, we use a random sample for simulation. The NN thus enables *active learning* by generating high-quality input samples until system requirements are met or the sampling budget is exhausted.

We summarize the major contributions of this article as follows.

- 1) We formulate system design as an MOO problem and propose ASSENT, a two-step method for sample-efficient system synthesis.
- 2) In step 1 of ASSENT, we explore a large discrete design space using GA and synthesize a coarse design. Exploring the entire search space helps avoid local minima. We terminate GA even if the design requirements are not met. Early termination helps avoid costly simulations.
- 3) In step 2 of ASSENT, we explore a continuous design space of component values to improve the value of the objective function. We use the saved simulations from step 1 to incorporate knowledge over the entire design space. We use an NN as a surrogate to model the system response. We use an MILP formulation of the NN to obtain an *inverse design* of the system. The MILP formulation builds on top of CNMA where we dynamically replace the design around which we search for possible solutions.
- 4) We demonstrate the efficacy of ASSENT on a wide array of design problems, ranging from nonlinear system design to circuit design. System design problems include Lunar lander [5], Acrobot [5], Polak3 [6], Waveglider [7], Rover path planning [8], and sensor placement for a power grid [9]. We show that ASSENT improves the value of the objective function in comparison to CNMA-based system synthesis by up to 53%. We also synthesize two-stage and three-stage transimpedance amplifiers and show that ASSENT attains a better value of the objective function compared to RL, BO, and human designs proposed in [10].

The remainder of this article is organized as follows. In Section II, we discuss related work. Section III provides the necessary background, followed by a simple motivational example in Section IV. In Section V, we introduce the methodology for sample-efficient nonlinear system design. We apply the methodology to the synthesis of nonlinear systems in Section VI. Finally, Section VII concludes this article.

II. RELATED WORK

In this section, we review previous works on solving MOO problems. We discuss weighted sum-based techniques like RL and BO, and then MOO using EAs. We also discuss the application of optimization techniques to system synthesis.

A. Optimization Techniques

The most commonly employed technique to solve MOO is formulating the optimization problem as a weighted sum of objectives. The weights are determined using domain expertise or through trial and error until given requirements are met. On the other hand, EAs like GA do not assume weights are provided for different objectives but yield a Pareto-optimal front that consists of solutions that trade off various objectives against each other.

1) *Weighted Sum Optimization*: BO uses gradient-free search to solve optimization problems based on an acquisition function that enables active learning. The acquisition function points to an input that needs to be simulated to obtain the corresponding system output. In turn, the input/output pair is used to update the acquisition function. Lyu *et al.* [11] exploited a disagreement among different acquisition functions to determine the next set of input points to simulate. Upper confidence bound [12] is another technique that is used to obtain the best tradeoff between exploitation and exploration when determining the next input for simulation.

Recent works use deep RL for solving MOO in a sample-efficient manner [10]. RL requires a definition of the reward function as a weighted sum of different objectives. A policy chooses an input sample for simulation based on past inputs and corresponding outputs. The recent interest spurt in using RL combined with deep learning is due to the approach presented in [13]. It is based on training a convolutional NN to learn a policy for playing Atari games. It was extended to the continuous action space in [14] to solve simulated physics tasks and learn end-to-end policies that are more sample-efficient than those discussed in [13].

2) *MOO*: EA is a widely used gradient-free search technique for obtaining Pareto-optimal solutions to an MOO problem. GA, a type of EA, is known to be suitable for such problems [15]. A seminal work in this field is the NSGA-II algorithm [16] that uses a fast nondominated sorting approach to reduce computational complexity by orders of magnitude. EAs have several variants, e.g., differential evolution that perturbs randomly selected population members based on the difference between selected individuals [17], swarm intelligence that includes ant colony optimization [18], and particle swarm optimization (PSO) [19]. Zhou *et al.* [20] built on PSO to develop an effective communication mechanism to solve MOO problems using a multitask multiview learning method. The sampling efficiency of GA is improved using surrogate models in [3]. Promising individuals are filtered using a Gaussian process-based surrogate model in the first level. The second level uses the radial basis function for gradient-based search.

B. System Synthesis

EA was widely used in the 1990s and early 2000s for the synthesis of electrical circuits [15]. The use of EA to obtain

the topology of analog circuits was pioneered in [21]. Parallel GA and circuit-construction primitives were used to create circuit graphs to evolve designs for an analog filter and amplifier in [22]. Synthesis of amplifiers and filters was done by solving constrained MOO with NSGA-II in [23]. A GA-based synthesis framework to simultaneously select the topology and perform component sizing for passive analog circuits was presented in [24]. In the first generation, certain component values are assigned *a priori*. During evolution, the crossover is conducted only on well-defined subcircuits to speed up GA convergence.

More recent works have primarily focused on determining component values for a fixed architecture. The method proposed in [10] uses deep deterministic policy gradient (DDPG), a form of RL, for the sample-efficient synthesis of two-stage and three-stage transimpedance amplifiers. The method in [25] proposes deep RL combined with transfer learning over a sparse design space to synthesize analog circuits. Canelas *et al.* [26] utilized a fuzzy *c*-means-based yield estimation method to reduce the number of Monte Carlo (MC) simulations for analog integrated circuits (IC) design. At each GA generation, the population is clustered and MC simulations are performed only on individuals representing the cluster. de Lima Moreto *et al.* [27] used Gaussian-profile-based fitness functions within EA formulations to improve the robustness of the solutions for analog IC design. Pattern search combined with EA is used in [28] for optimizing analog circuits. An automatic design exploration tool utilizing two different metaheuristics working concurrently is used for designing arithmetic-logic units in [29]. A GA-based constraint transformation method is used to prune the design search space in [30]. The circuit synthesis tool focuses on the pruned search space to make the design process efficient.

NN-based surrogate models are used to model nonlinear response to design Verilog-analog and mixed-signal blocks in [31]. Garitselov *et al.* [32] used a polynomial-based meta-model to optimize a figure of merit to design a ring oscillator. The conflicting objectives like power and frequency are converted into a single objective by taking their ratio. A physical design-aware NN is used in [33] to predict the response of a phase-locked loop (PLL). Artificial bee colony optimization is used in [33] to compute the response of the PLL using an NN instead of performing actual simulations to speed up synthesis. A memetic algorithm based on the bee colony algorithm and an NN is used to design analog circuits in [34].

Okobiah *et al.* [35] used a Kriging-based metamodel and simulated annealing to optimize CMOS-based sense amplifiers. The method in [11] uses BO with an ensemble of acquisition functions to tackle complex mathematical functions and synthesize electrical circuits. We instead rely on CNMA [4] that uses an MILP formulation of the NN for selecting component values to synthesize systems.

Table I shows a comparison of ASSENT with BO and EA. BO is sample-efficient but its complexity increases with an increase in the number of training instances. EA requires multiple simulations, making the design process sample-inefficient. The two-step synthesis makes the ASSENT sample-efficient. BO typically requires specifying the system design problem as a

TABLE I
COMPARISON OF SYNTHESIS METHODOLOGIES WITH ASSENT

	Bayesian optimization	Evolutionary algorithm	ASSENT
Sample-efficient	✓	×	✓
Independent constraint handling	×	✓	✓
Architecture discovery	×	✓	✓
Active learning	✓	×	✓
Inverse design	×	×	✓

weighted sum of objectives and constraints [11]. The weights are determined using domain expertise or a trial-and-error approach, making the design procedure inefficient. EA and ASSENT handle the objective and constraints independently. BO searches for component values for a fixed architecture. EA and ASSENT can be used for both architecture search and component selection. BO and step 2 of ASSENT use an active learning framework that helps make the design process sample-efficient. ASSENT uses inverse design for active learning in step 2. The designer specifies the desired outputs and the MILP solution determines the candidate solution. BO and EA generate candidate solutions using a forward design.

III. BACKGROUND

In this section, we discuss preliminary material that our work builds on. We discuss the formulation of system design as an MOO problem. Next, we discuss GA and its applicability to system architecture search. Finally, we give a brief review of CNMA for the inverse design of a system. The sister article [4] describes CNMA in great detail.

A. System Design Through Multiobjective Optimization

When designing a system, the designer is interested in achieving the desired objectives subject to given constraints. MOO is one of the ways to formulate this problem. The MOO solutions enable best tradeoffs among competing objectives. They constitute a *nondominated* set and lie on a surface called the *Pareto front* [36]. More formally, the system design problem is formulated as follows:

$$\begin{aligned}
 & \underset{\mathbf{x}, \mathbf{y}}{\text{minimize}} && f_m(\mathbf{x}, \mathbf{y}), && m = 1, 2, \dots, M \\
 & \text{subject to} && g_j(\mathbf{x}, \mathbf{y}) \geq 0, && j = 1, 2, \dots, J \\
 & && h_k(\mathbf{x}, \mathbf{y}) = 0, && k = 1, 2, \dots, K \\
 & && x_i^L \leq x_i \leq x_i^U, && i = 1, 2, \dots, n
 \end{aligned} \quad (1)$$

where \mathbf{y} represents the design space over all possible architectures or the ways components can be connected to form a system, \mathbf{x} is the design space over all possible component values, and $f_m(\mathbf{x}, \mathbf{y})$ is the m th objective. The system must also

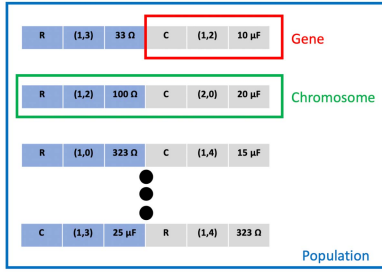


Fig. 1. Details of different elements of GA. Each component is color-coded (resistor in blue and capacitor in gray). Gene depicted in a red box, chromosome in a green box, and population in a blue box.

satisfy J inequality constraints given by $g_j(x, y)$ and K equality constraints given by $h_k(x, y)$. For instance, when designing a Lunar lander [5], the goal is to maximize the reward determined by the position at which the module lands subject to constraints on fuel consumption and time taken to land. The range of values of available components constrains the inputs. The lower bound for value x_i of component i is labeled as x_i^L and its upper bound as x_i^U .

B. Genetic Algorithm

System designs often rely on human expertise. However, this may lead to failure to find a design that meets all system requirements or require long simulation runs to explore the large design space. In the first step of ASSENT, we harness GA's exploration capability and ease of encoding an architecture [37] to solve an MOO formulation of system design. GA evolves a population of individual solutions through multiple generations. The main steps of GA are as follows.

- 1) Each individual in the first generation of a population is represented with a *chromosome*. A chromosome is a sequence of genes.
- 2) Each individual is evaluated based on how well it meets its objectives and constraints.
- 3) A subset of these individuals is selected to produce children for the next generation.
- 4) Pairs of randomly chosen individuals (parents) from this subset undergo reproduction using *crossover* by combining the genes of the parents to create children.
- 5) The genes of each child are *mutated* by perturbing them with low probability to facilitate exploration across various dimensions.
- 6) The best performing individuals in the current generation and the children (after step 5) are retained.
- 7) Steps 2–6 are repeated until one of the stopping criteria is met.

In ASSENT, a *chromosome* corresponds to a design choice for the complete system. The design choice may represent the system architecture and its component values or only the component values for a fixed architecture. A *gene* encodes details of a particular component, like its type, connecting nodes, and value. We evaluate the design through a simulator. We use tournament selection to select the individuals that undergo reproduction [38]. Fig. 1 shows a population of individuals, i.e., chromosomes, and genes. Here, the system architecture corresponds to an electrical circuit. The gene shown in the

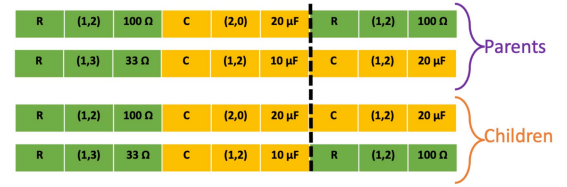


Fig. 2. Crossover operation to produce children from parents. Crossover point shown with a dotted line.

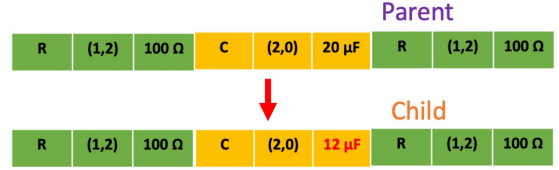


Fig. 3. Mutation of an individual. The capacitance changes from 20 to 12 μF . The changed value is shown in red.

red box depicts a capacitor with a capacitance of 10 μF connected between nodes 1 and 2. A sequence of genes forms a chromosome or an individual shown in the green box. The blue box shows the entire population within a generation. Fig. 2 shows the crossover operation. The dotted line shows the crossover point. The genes of the two parents are exchanged at the crossover point to produce children. Fig. 3 shows the mutation of an individual. The capacitance changes from 20 to 12 μF . The changed value is shown in red. GA requires many simulations to obtain a design that meets all the specifications, thereby pointing to the need for a sample-efficient design procedure.

C. Inverse System Design Using NN

We overcome the sample inefficiency of GA by terminating it at an intermediate stage (before necessarily reaching a valid or acceptable design) and then using a sample-efficient search method to meet system requirements. Akintunde *et al.* [39] proposed an MILP formulation of an NN with ReLU activation in the context of neural agent–environment systems to solve the problem of *reachability* through an NN-based policy trained using RL. Reachability indicates whether the NN can output the desired values using permissible inputs. An NN is converted into an MILP by representing all hidden neurons with constraints defined as follows:

$$C_i = \left\{ \begin{aligned} \bar{x}_j^{(i)} &\geq W_j^{(i)} \bar{x}^{(i-1)} + b_j^{(i)} \\ \bar{x}_j^{(i)} &\leq W_j^{(i)} \bar{x}^{(i-1)} + b_j^{(i)} + Q \bar{\delta}_j^{(i)} \\ \bar{x}_j^{(i)} &\geq 0, \bar{x}_j^{(i)} \leq Q(1 - \bar{\delta}_j^{(i)}), j = 1, \dots, L^{(i)} \end{aligned} \right\}. \quad (2)$$

In (2) $\forall i, j, \bar{x}_j^{(i)}$ corresponds to the j th neuron in the i th layer, $L^{(i)}$ is the number of neurons in the i th layer, $W_j^{(i)}$ represents weights that determine the input to $\bar{x}_j^{(i)}$, $\bar{x}^{(i-1)}$ represents outputs from the $(i-1)$ th layer, $b_j^{(i)}$ is the bias for neuron $\bar{x}_j^{(i)}$, Q is larger than the largest possible magnitude of $W_j^{(i)} \bar{x}^{(i-1)} + b_j^{(i)}$,

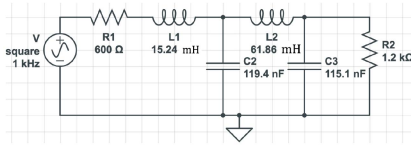


Fig. 4. Low-pass Butterworth filter architecture and component values used as a seed design.

and $\bar{\delta}_j^{(i)}$ is defined as follows:

$$\bar{\delta}_j^{(i)} \triangleq \begin{cases} 0, & \text{if } \bar{x}_j^{(i)} > 0 \\ 1, & \text{otherwise.} \end{cases} \quad (3)$$

The constraints imposed by the hidden neurons of the network are obtained from the union of all the constraints (C_i) shown in (2).

CNMA [4] uses the above formulation to determine the component values of a given system architecture with the aim of achieving the best value of the objective function. An NN predicts the output corresponding to the inputs by minimizing the mean-squared error (MSE) for all the simulated points. The designer specifies the constraints on the inputs and the desired output. The desired output corresponds to the objective function and the output constraints. The NN is converted into MILP using (2). A feasible solution to the MILP determines the component values required to perform the simulation. In the case of an infeasible solution, the system is simulated using a random sample. We change the desired output to gradually improve the value of the objective function while satisfying the constraints. Next, we illustrate ASSENT using a motivational example that involves designing a low-pass filter.

IV. MOTIVATION

We propose ASSENT as a solution to the nonlinear system design problem. We illustrate its working through the design of a low-pass filter. The objective is to obtain a *unity gain* (0 dB) and a *bandwidth* of 1 kHz while *minimizing* the number of circuit components. We first synthesize a coarse design in step 1 that is fine-tuned in step 2.

A. Coarse Design

We assume the following discrete components are available in step 1: 1) resistors [1, 10, 600, 1200] Ω; 2) capacitors [1e-12, 119.37e-9, 155.12e-9, 1e-5] F; and 3) inductors [1e-6, 10e-3, 15.24e-3, 61.86e-3] H. The seed design is a Butterworth low-pass filter adapted from [40] and shown in Fig. 4. We evolve it through GA till the point it gets close to meeting the specifications. We use a maximum of five nodes and ten components in the circuit architecture to expand the design space even though we know that a low-pass filter can be designed with just three nodes and two components (besides the supply). The total number of choices for a gene is given by $(\# \text{component types}) \times (\# \text{connecting points}) \times (\# \text{different component values}) = 3 \times 5^2 \times 4 = 300$ (each component has two connecting points resulting in 5^2 connecting points) [15]. In our example, since there may be ten components in the circuit, the design space size is 300^{10} . Hence, we need to search the large design space efficiently.

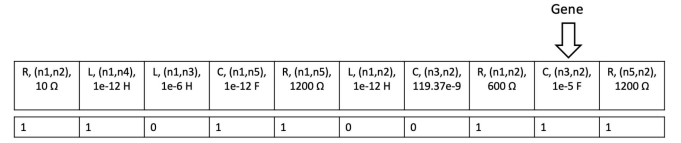


Fig. 5. Chromosome representation of a low-pass filter. The top row represents the details of all the ten components. It shows the component type given by (R, L, C) and its connecting nodes ($n1, n2, n3, \dots$) and value. The bottom row indicates whether the component is active (1) or inactive (0) in the circuit.

Fig. 5 shows the chromosome representation of a circuit. A gene encodes details of a component, including its type, connecting nodes, and value (shown in the top row). The bottom row shows whether the component is active (1) or inactive (0) [15]. We use the following objectives to find the coarse design by searching the architecture and component space using GA.

- 1) Weighted sum of the difference between the desired *magnitude* response of a first-order low-pass filter and the observed response. We set the weights in the *passband* to 40 and 1 in the *stopband* to give more importance to the response in the *passband*. Note that since GA synthesizes a coarse design, other values may work too. We use a weighted sum here to cover the entire frequency range.
- 2) Weighted sum of the difference between the desired *phase* response of a first-order low-pass filter and the observed response. The weights are the same as above.
- 3) Number of *active* components: a lower value implies fewer components.

We use GA for architecture search using 50 individuals comprising the seed design and other randomly generated individuals evolved over 100 generations. Fig. 6 shows the scaled mean (with respect to the seed design) of the three objectives for the entire population from the 10th generation onward. We plot the mean objective values after the 10th generation because the initial GA generations have very high objective values. The x -axis shows the generation number and the y -axis shows the mean value for the three objectives. Since the mean values are scaled, the y -axis has no unit. There is a tradeoff among the three objectives across generations, as evident from the figure. After 100 generations, we select a nondominated individual from the Pareto front based on the first two objectives (magnitude and phase). This individual (circuit) has a bandwidth of 966 Hz, the phase of -46° , a gain of 0 dB, and a total of three components. Since this is a coarse design, it does not meet the requirements yet. Fig. 7 shows the GA-evolved circuit. The circuit synthesized by GA can be simplified using human intervention by replacing the two parallel capacitors with a single equivalent capacitor, thus yielding a standard low-pass filter. The next step is to fine-tune the component values in a continuous design space.

B. Fine-Tuning

We perform fine-tuning through an NN with a hidden layer consisting of 100 neurons converted into an MILP. The NN inputs are component values (resistor and capacitor) derived from a feasible solution to the MILP or a random sample if a

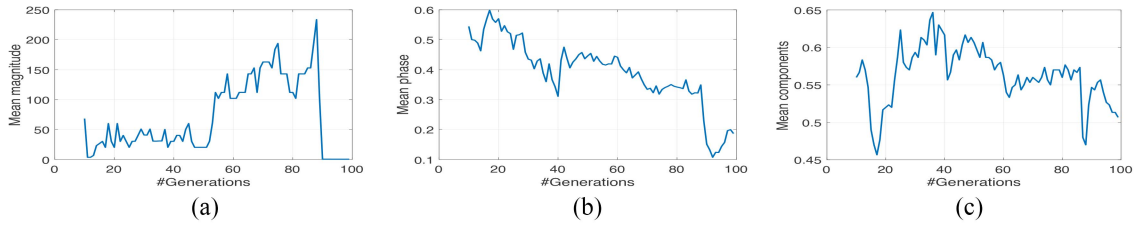


Fig. 6. Scaled mean objectives across all individuals in a generation for (a) magnitude, (b) phase, and (c) component values from the 10th generation onward for architecture search for low-pass filter design.

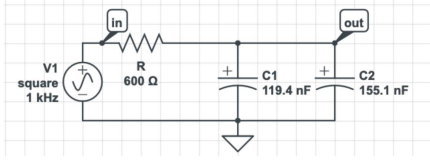


Fig. 7. Low-pass filter architecture evolved by GA.

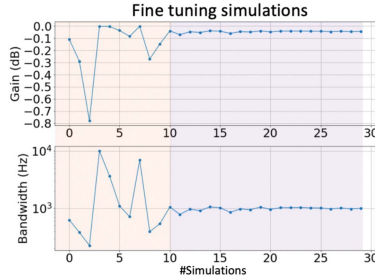


Fig. 8. Gain and bandwidth during fine-tuning using step 2.

feasible solution does not exist. The continuous design space is $[400, 800]\Omega$ for resistor and $[0.01, 1]\mu\text{F}$ for capacitor. Since this is a simple design, through prior knowledge, we know that a low-pass filter can be synthesized within these ranges of component values to meet the specifications. The targeted outputs of the NN are gain, bandwidth, and response of the filter at 200, 500, and 2000 Hz. The responses at these frequencies sufficiently capture the behavior of the filter below and above the desired bandwidth. The output constraints are as follows: gain (from input to output) in the range $[-0.92, 0.83]$ dB and bandwidth in the range $[990, 1010]$ Hz. We generate ten random input samples to initialize the NN for training to minimize the mean squared error (MSE). The solutions suggested by MILP meet the requirements after 20 more simulations. We show these simulations (10 for initialization of the NN and 20 during the MILP step) in Fig. 8: initialization points in the orange part and MILP ones in the blue part. The outcomes during initialization are random as they are far from meeting the requirements. However, the points suggested by the MILP have a response closer to the requirements until finally, the suggested point meets the specification. Fig. 9 shows the component values on termination of step 2.

V. SYNTHESIS METHODOLOGY

In this section, we describe ASSENT in detail. The first step explores a large design space using GA. The outcome of the first step is a *coarse* design that is fine-tuned in step

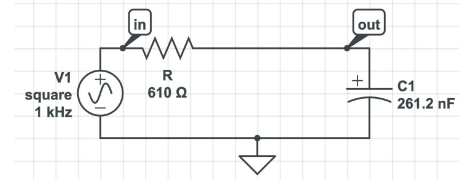


Fig. 9. Low-pass filter architecture (after human intervention on the GA schematic) at the end of the second step.

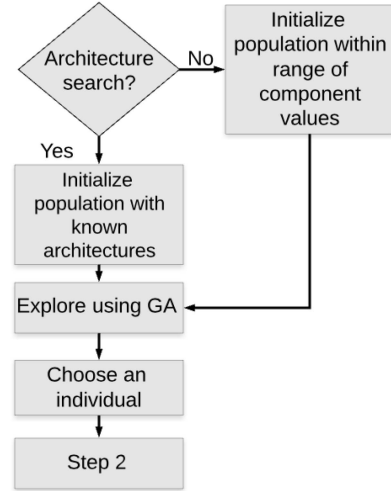


Fig. 10. Evolution using GA.

2 using a sample-efficient search to obtain component values that satisfy all the constraints and try to improve the value of the objective function obtained in step 1.

A. Step 1: Coarse Design

Design of systems with multiple choices for architectures and component values requires search in a large design space. We achieve this through GA mainly due to its ease of encoding architectures and component values. GA also helps in exploring the entire design space, thus avoiding local minima. We discretize the large design space to obtain a coarse design. The coarse design may even violate hard constraints or attain an inferior value of the objective function compared to other synthesis methodologies.

We show the flow involved in the synthesis of the coarse design in Fig. 10. We evolve individuals across generations using NSGA-II [16] that yields nondominated solutions of the system design formulated as an MOO problem. ASSENT only requires a coarse design in step 1. Hence, any MOO

Algorithm 1 Step 1: Architecture Synthesis Using GA

Input: S : Seed design(s); N : #generations; P : population size; C : Components; R : Component range; *nodes*: Nodes; *max_comp*: Max # components; *stop*: Stopping criteria; B : buffer to store simulations; *mut*: mutation probability; *cross*: crossover probability

- Generate *Sobol* samples for C within R
- Initialize individuals with S and others randomly

while not *stop* **do**

- Compute *objectives* for all P
- Store input and the corresponding output in B
- Rank P using *NSGA-II*
- Use tournament selection to create mating population of size P
- Use reproduction based on *crossover* and *mutation* to create P children
- Select P from $2P$ members using *NSGA-II*

end while

Output: Best individual from the final generation using a metric, and buffer B

design exploration tool such as NSGA-III [41] could also be used instead. In architecture search, we initialize some individuals in the first GA generation with seed design(s) from the literature to exploit prior knowledge. When performing only component selection, we initialize the individuals in the first generation with component values to cover the design space. This enables comparisons with other designs from the literature that do not use prior knowledge.

During *architecture search*, a *gene* has three constituents: type of component, nodes connecting the component, and the component value, as shown in Fig. 5. In the case of *component selection*, the gene encodes the value of the component in the *chromosome* that represents the circuit.

Algorithm 1 describes architecture search using GA. We generate P individuals in a generation. Some of these are from seed designs (S) and others randomly generated. We generate random individuals by selecting a random component, choosing the number of *nodes* (e.g., a resistor requires two nodes and a MOSFET requires three nodes) connected to that component, and the component value. We select the component values for random individuals from quasirandom *Sobol* samples in the range (R) of each component. Sobol samples are distributed uniformly over a unit hypercube [42]. Then we scale the samples to lie within the specified range for each component. We post-process individuals to ensure that some components connect to the fixed terminals of the architecture, e.g., *ground*, *supply voltage*, and *input/output terminals in the case of a circuit*, to ensure a valid design. We simulate all individuals in a generation to compute the objective functions. We handle constraints on the output by converting them into objectives. If the simulation is expensive, we utilize multiple cores and run GA in parallel. We store all the simulations in a buffer B to be used in step 2, if necessary. We also use the buffer as a lookup table in case the same design needs to be simulated again in step 1. Next, we rank

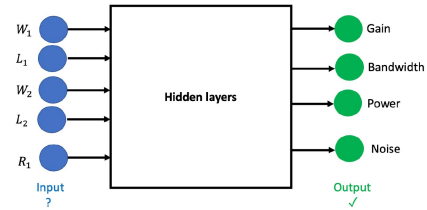


Fig. 11. Overview of the inverse design used in step 2.

the individuals using the *NSGA-II* algorithm [16]. We use tournament selection for selecting some individuals in a generation to undergo reproduction through *crossover* with a probability of *cross* and *mutation* with a probability of *mut* to produce P children. We use *NSGA-II* again to select P individuals out of the $2P$ individuals for the next generation. This process continues until one of the stopping criteria (*stop*) is met. These criteria are based on individuals not improving over a fixed number of generations, exhausting the simulation budget, or on attaining the required performance. Finally, we select one individual from the final generation based on a performance metric. The metric (lower the better) in our case is one of the multiple objectives or constraints. We select an individual from the last generation since ranking using *NSGA-II* ensures that we never lose an individual from the Pareto front within a generation. We select only one individual since GA only synthesizes a coarse system design, although it is also possible to select another individual to undergo fine-tuning in the next step.

Component selection for a fixed architecture uses a setup similar to Algorithm 1. Instead of initializing some individuals in the first generation by seed designs, we initialize all the individuals using Sobol samples. The rest of the procedure remains the same.

B. Step 2: Fine-Tuning

The design obtained from step 1 may not always meet the hard constraints. Even if it meets the hard constraints, it is possible to improve the value of the objective function by searching in a continuous design space. When using step 1 for architecture search, we use human intervention to refine the synthesized design if needed. We fine-tune this design through a modified version of CNMA [4] by searching in a continuous space. In contrast to CNMA where the component selection stops on exhausting the simulation budget, we adaptively replace the design from step 1 to improve the value of the objective function. Step 2 yields one candidate solution in each iteration using an active learning framework. Fig. 11 shows a high-level overview of this step through an example. The designer specifies the system requirements shown on the right in green. The feasible solution of the MILP determines the potential component values shown on the left in blue that achieve the desired response.

Fig. 12 shows the procedure to fine-tune the design that step 1 yields. In the flowchart, N denotes the number of simulations in a particular trial out of a total of T trials. We effectively repeat the fine-tuning step T times, allowing a maximum of N valid simulations in a trial. We consider a simulation to be

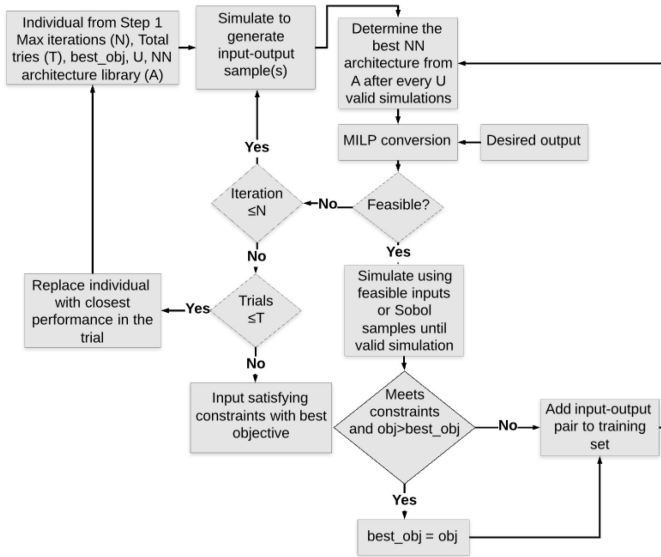


Fig. 12. Flowchart that illustrates the fine-tuning procedure in step 2 of ASSENT.

invalid if the output from the simulator yields an error. We represent the best value of the objective attained from step 1 by *best_obj*. Next, we generate *Sobol* samples from the range of each component in the design from step 1, followed by simulation of these points to determine their outputs. We generate samples around the nominal values of each component (e.g., $\pm 70\%$ of $10\ \Omega$ for resistor). We clip the samples to ensure that the component values are within the permissible range. We model the response of the system to the inputs using an NN. We either pretrain the NN using the simulations saved from step 1 and the *Sobol* samples or only on the *Sobol* samples generated around the best design determined from step 1. We use the simulations saved from step 1 to obtain a better value of the objective function in fewer samples. However, this is not suitable for some systems where the number of samples required may be higher to overcome the inductive bias since step 1 searches over the entire design space. We select the best NN from an NN architecture library that yields the least MSE on the validation set. We update the NN architecture after every *U* valid simulation. We convert the NN into an MILP using (2) to see if there is a feasible solution. We determine the constraints from the *desired output* of the system. The range of available components determines the constraints on the input. We use Gurobi [43] to find a feasible solution to the MILP problem. If such a solution exists, it indicates that the desired output is reachable by the NN from this input. We simulate the system with the suggested input. If the simulation is invalid, we use *Sobol* samples until a valid simulation output is obtained. We update *best_obj* when the value of the objective function improves. We then add the input–output pair corresponding to the feasible solution to the training set. If the solution to the MILP problem is infeasible, we generate a *Sobol* sample and add the corresponding output to the training set. The procedure continues until a maximum number of permissible simulations (*N*) is exhausted.

After finishing a trial, the input corresponding to the least absolute sum in terms of fractional deviation of the

output from the requirement replaces the design from step 1. Fractional deviation is computed as follows:

$$\sum_i \frac{|\text{obs}_i - \text{spec}_i|}{\text{spec}_i} \mathbb{1}_{\{\text{obs}_i \leq \text{spec}_i\}} \quad (4)$$

where spec_i is the specification for the *i*th objective or constraint and obs_i is the observed response of the system for the *i*th objective or constraint. $\mathbb{1}_{\{\text{obs}_i \leq \text{spec}_i\}}$ is an indicator function that takes the value 1 in the case of violation of spec_i determined by obs_i (can be greater or less than) and 0 otherwise. After the last trial, we return the input that corresponds to the output that satisfies all the hard constraints and yields the best value of the objective function.

C. Discussion

The complexity of step 1 of the algorithm is $O(n)$, where *n* is the number of calls to the simulator. Step 2 complexity is linear in the number of training instances required for the NN. Note that BO, against which comparisons are made in the sister Part I of this article as well as for circuit synthesis later in this article, has a $O(n^3)$ surrogate-building complexity in the number of samples. The MILP formulation is efficiently solved with industrial-strength MILP solvers, such as Gurobi [43].

VI. EXPERIMENTAL RESULTS

In this section, we first illustrate how ASSENT can be used for component selection in the design of the following benchmarks: Lunar lander [5], Acrobot [5], Polak3 [6], Waveglider [7], Rover path planning [8], and sensor placement for a power grid [9]. We also use ASSENT to synthesize electrical circuits for two cases. In the first case, we use ASSENT for architecture search and component selection to design a circuit that achieves the functionality of a two-stage transimpedance amplifier. In the second case, we select the component values for a fixed architecture for two-stage and three-stage transimpedance amplifiers. We implement ASSENT using Keras [44], Scikit-learn [45], Gurobi [43], and PyGMO [46]. The simulations are performed on an Intel Xeon processor with 64 GB of DRAM.

A. Component Selection for System Design

We illustrate the selection of component values on various benchmarks and compare their performance to that of designs obtained using CNMA [4] with 1, 5, and 10 solvers. We only provide a comparison with CNMA as it yields the best value of the objective function relative to other optimization techniques [4].

Lunar Lander: The goal is to maximize the reward obtained by the landing position subject to constraints on the fuel used and the time taken to land. We run step 1, i.e., GA for component selection with 100 individuals for a maximum of 400 generations. We set the crossover probability (*cross*) to 0.9 and mutation rate (*mut*) to 0.1 that are typical values for GA. We terminate step 1 if any of the following stopping criteria are met: 1) reward is above 500; 2) after the 10th generation, the objective value for reward does not improve for ten generations; or 3) we reach the maximum number of generations. We

TABLE II
COMPARISON OF REWARD USING CNMA AND
ASSENT FOR LUNAR LANDER

Procedure	# Simulations	Total time	# Initial samples	fuel ≤ 75	time ≤ 10	reward
CNMA-1	2,066	1,500s	100	34.12	2.60	437.1
CNMA-5	1,358	1,500s	100	59.91	2.88	469.6
CNMA-10	1,494	1,500s	100	43.35	3.92	465.1
Step 1	1,400	42s	-	52.59	2.64	451.4
Step 2	583	54,000s	1	47.09	3.50	475.7

convert the constraints into objectives in step 1 and formulate the problem as an MOO. There are three objectives in step 1 described next.

- 1) Objective for fuel consumption

$$\left(\frac{F_{\text{meas}}}{F_{\text{max}}} + \alpha \frac{F_{\text{meas}} - F_{\text{max}}}{F_{\text{max}}} \right) \mathbb{1}_{\{F_{\text{meas}} > F_{\text{max}}\}} \quad (5)$$

where α is set to 15 and represents the penalty for fuel consumption (F_{meas}) when it exceeds the maximum permissible value (F_{max}), which is 100 units in our case. $\mathbb{1}_{\{F_{\text{meas}} > F_{\text{max}}\}}$ is an indicator function that takes a value of 1 when $F_{\text{meas}} > F_{\text{max}}$, and 0 otherwise.

- 2) Objective for the time taken to land is defined in the same way as fuel consumption. The maximum time allowed for landing is ten units.
- 3) Objective for reward is defined as

$$\frac{400}{\text{reward}_{\text{attained}}} \mathbb{1}_{\text{reward}_{\text{attained}} > 0} + (\text{abs}(\text{reward}_{\text{attained}}) + 1000) \mathbb{1}_{\text{reward}_{\text{attained}} \leq 0} \quad (6)$$

where $\text{reward}_{\text{attained}}$ is the reward for a particular choice of component values. As we need to maximize the reward, the lower the value of (6), the better is the design. The first term in (6) yields a lower value of the objective for a higher reward. We choose 400 as the numerator since it is close to the reward attained using sequential CNMA (437.1). The second term corresponds to the case for negative reward. We set this term to a large number to penalize designs with a negative reward.

In case of simulation that does not lead to success, we set the objective values to a very large number to indicate this fact.

Table II shows the rewards and constraints for the designs obtained using CNMA and ASSENT. In the table, CNMA-1, CNMA-5, and CNMA-10 refer to CNMA runs based on 1, 5, and 10 solvers, respectively, [4]. Step 1 requires less time compared to CNMA, since GA does not need to solve the time-consuming MILP formulation after simulation.

In step 2, we aim to improve the reward further. We set the number of trials (T) to 50, the maximum number of iterations (N) to 20 in the first trial, and 50 from the second trial onward. We terminate step 2 at the end of 15 h. We use all the simulations saved from step 1 with a reward greater than 400 to narrow down to a promising part of the design space. We generate Sobol samples within $\pm 70\%$ of the design attained in step 1. Since we use the simulation results from step 1, we generate only one additional Sobol sample in each trial. We set the update frequency (U) of the NN architecture search to 10. We select an NN with one of the following architectures (A):

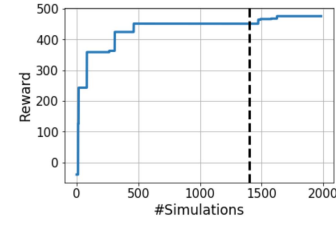


Fig. 13. Reward versus the number of simulations for Lunar lander in step 1 (2) to the left (right) of the dotted line.

TABLE III
COMPARISON OF $t_{\text{stabilize}}$ USING CNMA AND ASSENT FOR ACROBOT

Procedure	# Simulations	Total time	# Initial samples	$t_{\text{stabilize}}$ (s)
CNMA-1	247	1.4 hrs	20	3.4
CNMA-5	285	1.4 hrs	20	3.2
CNMA-10	520	1.4 hrs	20	2.8
Step 1	1,386	2.8 hrs	-	3.0
Step 2	1,359	15 hrs	1	2.6
Step 2- tight bound	1,293	15 hrs	1	2.4

[(40, 20, 8), (30), (15), (100), (50), (200), (20, 20, 8), (300), (400), (500), (600)], where the tuples represent the number of neurons in the hidden layer(s). The NN inputs represent component values and the outputs represent fuel consumption, time taken to land, and reward. We use a *multilayer perceptron regressor* from the Scikit-learn [45] package along with the Adam optimizer [47], an initial learning rate of 0.0001, *adaptive* learning, and a *maximum iteration count* of 100 000 to train the NN. We set other parameters to their default values. Unless otherwise specified, we use the same setup for all the experiments.

The last row of Table II shows the reward attained after fine-tuning. Step 2 requires more time than taken by CNMA, primarily due to the time required for NN architecture search and due to the different system configurations used to run the experiments. We improve the value of the reward from 451.4 to 475.7. Fig. 13 plots the highest reward attained versus the number of simulations. To the left of the dotted line is the reward attained in step 1 and to the right is the reward attained in step 2. We observe that fine-tuning helps further improve the reward.

Acrobot: The objective is to minimize the time required to stabilize ($t_{\text{stabilize}}$) the system by selecting the design parameters for the two arms of the Acrobot. We terminate GA if $t_{\text{stabilize}}$ falls below 3.2 s. Other stopping criteria are the same as the ones used in the Lunar lander example. Table III shows a comparison of $t_{\text{stabilize}}$ attained using CNMA and ASSENT. Step 1 yields a design with $t_{\text{stabilize}} = 3.0$ s.

In step 2, we fine-tune the component values to further reduce $t_{\text{stabilize}}$. We use all the simulations saved in step 1 with $t_{\text{stabilize}} \leq 5.0$ s. We select an NN with one of the following architectures (A): [(10), (15), (20), (30), (100)]. We reduce the value of $t_{\text{stabilize}}$ to 2.6 s. We further explore if tightening the bounds within which we generate the inputs to $\pm 20\%$ from $\pm 70\%$ of the nominal design from step 1 can reduce $t_{\text{stabilize}}$. These results are shown in the last row of Table III. The modified setup yields a design with $t_{\text{stabilize}}$ equal to 2.4 s.

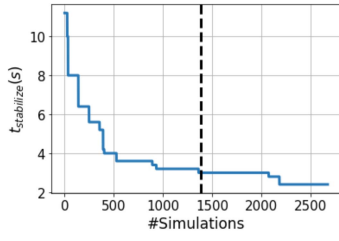


Fig. 14. $t_{\text{stabilize}}$ versus the number of simulations for Acrobot in step 1 (2) to the left (right) of the dotted line.

TABLE IV
COMPARISON OF V_{Boat_x} USING CNMA AND ASSENT FOR WAVEGLIDER

Procedure	# Simulations	Total time	# Initial samples	V_{Boat_x}	V_{Boat_y}	f_{Glider_x}
CNMA-1	1,920	0.69 hr	30	3.90	2.286	107.53
CNMA-5	3,170	0.69 hr	30	3.90	2.286	107.48
CNMA-10	3,920	0.69 hr	30	3.90	2.286	107.48
Step 1	2,145	0.37 hr	-	3.61	2.286	248.83
Step 2	2,383	15 hrs	1	3.90	2.286	108.95

Fig. 14 plots the best value of $t_{\text{stabilize}}$ versus the number of simulations.

Waveglider: The objective in this benchmark is to maximize V_{Boat_x} subject to the constraints $|f_{\text{Boat}_x} - f_{\text{Glider}_x}| \leq 0.05 * f_{\text{Boat}_x} \wedge V_{\text{Boat}_x} \geq V_{\text{Boat}_y}$. Here, f_{Boat_x} (f_{Glider_x}) is the force of the boat (glider) and V_{Boat_x} (V_{Boat_y}) is the velocity of the boat in the x (y) direction. The component values represent the dimensions of the boat and hydrofoil. We define the following objectives for GA.

- 1) Objective corresponding to the deviation between f_{Boat_x} and f_{Glider_x}

$$\left(\text{con}_1 + \alpha \frac{\text{con}_1 - 0.05}{0.05} \right) \mathbb{1}_{\text{con}_1 \geq 0.05} \quad (7)$$

where $\text{con}_1 = [(f_{\text{Boat}_x} - f_{\text{Glider}_x}) / (f_{\text{Boat}_x} + 1e^{-12})]$, and $\alpha = 15$.

- 2) Objective corresponding to $V_{\text{Boat}_x} \geq V_{\text{Boat}_y}$

$$(\text{con}_2 - \alpha \text{con}_2) \mathbb{1}_{\text{con}_2 \leq 0} \quad (8)$$

where $\text{con}_2 = V_{\text{Boat}_x} - V_{\text{Boat}_y}$.

- 3) The third objective is $-V_{\text{Boat}_x}$. We reverse the sign as we need to maximize the velocity of the boat in the x direction.

Table IV shows the value of V_{Boat_x} obtained using CNMA and ASSENT. Step 1 terminates after 2145 simulations in 0.37 h due to saturation in performance.

In step 2, we use all the valid simulations from step 1 to train the NN. We select an NN with one of the following architectures (A): [(10), (15), (20), (30), (100)]. Besides the three outputs from the simulator, we add an additional output when training the NN. This output is an identity mapping of f_{Boat_x} . It simplifies the MILP formulation by transferring the constraints to the NN output. We do not range-normalize the outputs to keep f_{Boat_x} and f_{Glider_x} to the same scale. We also increase the learning rate to 0.1 to speed up training. The design synthesized at the end of step 2 meets all the constraints and improves the value of V_{Boat_x} to 3.90 m/s. Fig. 15 plots the best value of V_{Boat_x} versus the number of simulations.

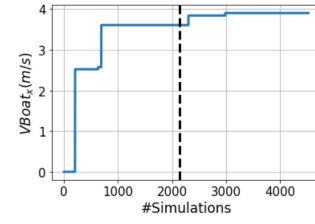


Fig. 15. Best value of V_{Boat_x} versus the number of simulations for Waveglider in step 1 (2) to the left (right) of the dotted line.

TABLE V
COMPARISON OF OBJECTIVE USING CNMA AND ASSENT FOR POLAK3

Procedure	# Simulations	Total time	# Initial samples	Objective
CNMA-1	859	2,000s	20	5.97
CNMA-5	1,970	2,000s	20	6.06
CNMA-10	2,700	2,000s	20	5.98
Step 1	37,397	72s	-	5.94

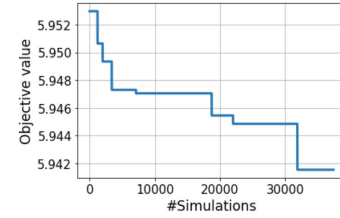


Fig. 16. Best value of the objective function in step 1 versus the number of simulations for Polak3.

Polak3: The objective is to minimize the maximum value of ten different transcendental functions. There are 11 inputs that represent component values. The objective of GA is to find the maximum value of the transcendental functions.

As simulations are not time-consuming for this problem, we let GA run serially for 400 generations. Step 1 requires a total of 37,397 simulations in 72 s, as shown in Table V. We attain an objective value of 5.94 compared to 5.97 obtained using CNMA. Our solution is closer to the known minimum value of 5.93 for this problem. Fine-tuning using step 2 does not improve the value of this objective. This indicates that if the simulations are cheap, step 1 may alone be sufficient to solve the optimization problem without the need of fine-tuning in step 2. Fig. 16 plots the value of the objective function versus the number of simulations.

Rover Path Planning: The objective is to find a trajectory that minimizes a cost function by selecting 30 2-D points that define the trajectory. We use this cost function as the objective for GA. We let GA run for 400 generations since the simulations are not time-consuming. Step 1 requires a total of 40 000 simulations in 201 s, as shown in Table VI. We obtain an objective value of 0.369 compared to 0.778 obtained using CNMA. Fine-tuning using step 2 does not improve the value of this objective further. Fig. 17 plots the best value of the objective versus the number of simulations.

IEEE 118 Bus Sensor Placement: The objective is to obtain the sensor placement such that sensor readings give the best chance of predicting the line failure pattern. The failure pattern is determined by the “ambiguity” in the sensor pattern. The

TABLE VI
COMPARISON OF COST FUNCTION USING CNMA AND
ASSENT FOR ROVER PATH PLANNING

Procedure	# Simulations	Total time	# Initial samples	Cost
CNMA-1	1,848	9,000s	2	1.148
CNMA-5	2,639	9,000s	2	0.997
CNMA-10	4,454	9,000s	2	0.778
Step 1	40,000	201s	-	0.369

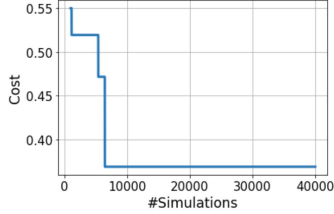


Fig. 17. Lowest cost versus the number of simulations from the 1000th simulation onward in step 1 for Rover path planning.

TABLE VII
COMPARISON OF AMBIGUITY USING CNMA AND ASSENT
FOR THE IEEE 118 BUS PROBLEM

Procedure	# Simulations	Total time	# Initial samples	Ambiguity
CNMA-1	251	1,500s	30	0.04813
CNMA-5	490	1,500s	30	0.02139
CNMA-10	380	1,500s	30	0.02139
Step 1	1,500	1,058s	-	0.01070

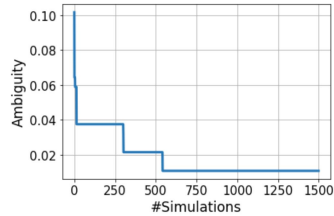


Fig. 18. Best value of the ambiguity in step 1 versus the number of simulations for the IEEE 118 bus problem.

maximum number of sensors is 50. We define the following two objectives for GA.

- 1) The first objective is to capture the constraint on the number of sensors

$$(\text{sensors}_{\text{used}} - 50) \mathbb{1}_{\text{sensors}_{\text{used}} > 50} \quad (9)$$

where $\text{sensors}_{\text{used}}$ denotes the number of sensors used in a particular configuration. We apply a penalty of $\alpha = 15$ when using more than 50 sensors.

- 2) The second objective is to minimize ambiguity as determined by the simulator output.

Step 1 terminates after 1500 simulations due to saturation in performance for ten generations. Table VII shows that step 1 achieves an ambiguity of 0.0107 in 1500 simulations. The ambiguity is lower by about 50% than the ambiguity attained using CNMA. Fig. 18 plots the value of ambiguity versus the number of simulations.

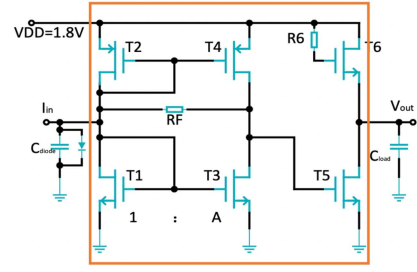


Fig. 19. Two-stage transimpedance amplifier from [10]. Component values are selected for devices inside the orange box and the values for those outside are fixed.

B. Circuit Design

In this section, we evaluate how ASSENT performs architecture search and component selection for electrical circuits. We compare our results with those in [10] that are synthesized by humans, RL, and BO. The technology files that specify the device physics for simulation are from [48] and are the same as in [10].

1) *Architecture Search and Component Selection*: We use the standard design of a two-stage transimpedance amplifier presented in [10] as the seed design for our methodology to take advantage of prior human knowledge. Fig. 19 shows this seed design. The objectives are to maximize the amplifier's bandwidth and minimize the sum of MOSFET gate areas in the circuit while satisfying hard constraints on *noise*, *gain*, *peak-ing*, and *power*. The design space comprises three components: two types of MOSFETs (pMOS and nMOS) and resistor. In the human-designed circuit, the MOSFETs are of minimum length ($0.18 \mu\text{m}$), based on the technology used, whereas the width is variable. Our search also uses minimum-length MOSFETs and only selects their width. We discretize the design space during architecture search (step 1) by generating 100 Sobol samples for resistors in the $[50, 5 \text{ k}]\Omega$ range and width in the $[0.18, 80]\mu\text{m}$ range. In the human-designed circuit, the resistor values are 420Ω and $3 \text{ k}\Omega$, and the width is in the $[0.9, 51]\mu\text{m}$ range. During GA evolution, we allow the circuit to have a maximum of 11 nodes and a total of ten components, whereas the seed design has six nodes and eight components, to enable search for novel designs. Since we need to represent ten components in a chromosome, we initialize two additional genes as resistors with a small resistance of $2.2 \mu\Omega$ whose terminals are shorted and not connected to any of the nodes in the seed design. This ensures the response of the seed design remains unaffected.

We use GA to evolve a generation of 100 individuals and set the maximum number of generations to 200. We choose these numbers to achieve at least about 50% sample efficiency (i.e., 50% fewer simulations) compared to the design methodology in [10]. We simultaneously search for the architecture and the component values, whereas the method in [10] only searches for component values. Hence, our method searches through a much larger design space, albeit with the seed design. We formulate an MOO problem with three objectives: 1) bandwidth; 2) noise; and 3) power. The objectives are described next.

- 1) *Bandwidth*: This objective corresponds to the weighted sum of the absolute difference between the desired

and observed responses, with a passband weight of 40 and a stopband weight of 1. We use the following reward/penalty.

- a) Assessing the level of reward/penalty is based on the operating region of each MOSFET: reward for MOSFET operating in the saturation region, else a penalty. We use a reward of 1 for operation in the saturation region. We apply a penalty of 2 (3) for operation in the linear (cutoff) region. We sum the rewards and penalty for each MOSFET and divide by the number of MOSFETs.
 - b) A penalty of 15 is assessed based on the fractional deviation in gain below 58.1 dB (since 58.1 dB is the gain achieved by RL-based synthesis in [10]).
 - c) A penalty of 15 is assessed based on the fractional deviation in peaking above 0.963 (achieved by RL in [10]).
 - d) A penalty of 15 is assessed based on the fractional deviation in bandwidth below 5.81 GHz (this is slightly higher than the bandwidth achieved by RL in [10]: 5.78 GHz). We scale the bandwidth objective by dividing it by the objective of the seed design.
- 2) *Noise*: This objective corresponds to the ratio of measured noise and the noise achieved by the RL-based design in [10] (19.2 pA/ $\sqrt{\text{Hz}}$). An additional penalty of 15 is assessed based on the fractional deviation in noise above this value.
 - 3) *Power*: This objective corresponds to the ratio of measured power and the power achieved by the RL-based design in [10] (3.18 mW). No penalty is assessed in this case due to the large room for optimization available for power consumption.

The objective for noise is given by

$$\frac{N_m}{N_{\text{ref}}} + \alpha \frac{N_m - N_{\text{ref}}}{N_{\text{ref}}} \mathbb{1}_{\{N_m > N_{\text{ref}}\}} \quad (10)$$

where N_{ref} is the noise of RL-designed circuit, N_m is the measured noise, and $\alpha = 15$ is the penalty. Other objectives are defined analogously.

We club together all the subobjectives related to bandwidth (gain, desired bandwidth, and peaking) into one to minimize the number of objectives that need to be tackled while capturing the entire frequency response. The penalty terms encourage the target response to be better than the response of the designs in [10]. In case the simulation is unsuccessful, we set the objective values to a very large number to indicate this fact.

We use a tournament size of 10, the mutation rate of 0.1, and crossover probability of 0.9, same as before. The evolution stops when one of the following criteria is met.

- 1) The scaled bandwidth objective falls below 0.9 since the aim is to improve it by about 10% relative to that of the seed design.
- 2) The number of generations exceeds 100 and the bandwidth objective stays the same for more than 100 generations, indicating saturation in GA performance.
- 3) The maximum number of generations (200) is reached.

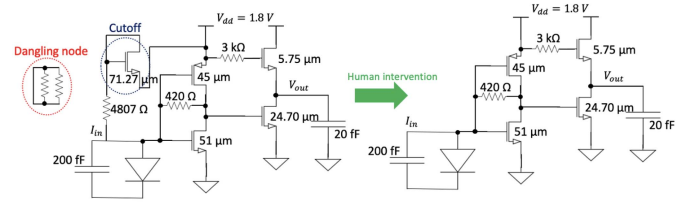


Fig. 20. Circuit synthesized by GA followed by human intervention. All MOSFETs are of minimum length (0.18 μm).

We choose the circuit with the best value of the objective for bandwidth as the coarse design in step 1 since this circuit addresses several subobjectives. We fine-tune the coarse design to meet the specifications in the next step. We remove dangling nodes through human intervention as they are redundant. We also remove a MOSFET operating in the cutoff region as it does not contribute to gain. Fig. 20 shows the circuit before and after human intervention. Table VIII shows the values of objectives and constraints before and after human intervention. The row named ASSENT step 1 shows the results before human intervention. GA requires less than an hour for synthesis. The second last row shows the results after human intervention. After the human intervention, the circuit does not meet the hard constraint for peaking. We remedy the constraint violation in step 2. The seed design has six MOSFETs. This one uses only four MOSFETs.

In step 2, we fine-tune the component values to maximize the bandwidth while satisfying all the hard constraints. We use a slightly modified setup for step 2 than in Section VI-A. Rather than using all the simulations saved from step 1, we initialize the NN using only Sobol samples around the design from step 1. We use 20 Sobol samples for initialization in the first trial and 1 Sobol sample in each subsequent trial. We empirically found that using the simulations saved from step 1 yields inferior results. We attribute this to the inductive bias imposed in step 1 due to sampling over the entire design space. Sobol samples around the design synthesized in step 1 enable focus on the region of interest. In all the experiments on electrical circuits, we select an NN with one of the following architectures (A): [(10), (50), (40, 20, 8)]. We let step 2 run until 50 trials are over with the other setup being the same, as described in the previous section.

Table VIII² shows a comparison of the design synthesized by ASSENT with designs obtained by humans, DDPG, and BO [10]. The last row depicts a design that satisfies all the hard constraints while maximizing bandwidth. We set the required area to less than $0.9\times$ of the human design when maximizing bandwidth. ASSENT synthesizes a design with a bandwidth of 6.18 GHz in 4239 simulations. It is about $12\times$ more sample-efficient than DDPG and achieves a much higher bandwidth. ASSENT requires a total of 25.4 CPU hours, whereas DDPG requires 30 GPU (type not specified) hours [10]. Fig. 21 plots the best value of bandwidth versus the number of simulations. We only plot the results for step 2 to show component selection results for a fixed architecture.

²The gate area is shown only for designs for which this information is available. There was a problem in area calculation in [10] that was confirmed after contacting the authors.

TABLE VIII
COMPARISON OF CIRCUITS SYNTHESIZED WITH ASSENT AND DESIGNS IN [10] (HARD CONSTRAINT VIOLATIONS SHOWN ENCIRCLED)

Spec.	#Samples	Time	Noise (pA/ $\sqrt{\text{Hz}}$)	Gain (dB Ω)	Peaking (dB)	Power (mW)	Gate area (μm^2)	Bandwidth (GHz)
Human Design [10]	1,289,618	months	≤ 19.3	≥ 57.6	≤ 1	≤ 18	-	maximize
DDPG [10]	50,000	30 GPU hrs	19.2	58.1	0.963	3.18	-	5.78
Bayesian Opt. [10]	880	30 hrs	19.6	58.6	0.629	4.24	-	5.16
ASSENT Step 1	1,600	0.15 hr	18.0	58.0	0.913	7.97	35.59	5.93
ASSENT Step 1+Human	-	-	17.9	58.0	1.042	7.97	22.76	5.96
ASSENT Step 1+2	4239	25.4 hrs	19.3	57.6	0.974	6.74	20.24	6.18

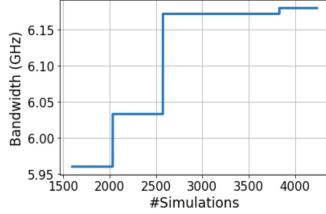


Fig. 21. Best bandwidth versus the number of simulations in step 2 when selecting component values for the architecture obtained using step 1 for the two-stage transimpedance amplifier.

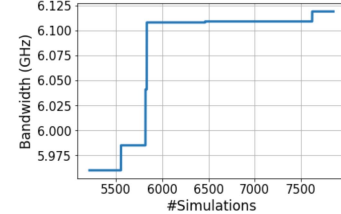


Fig. 22. Number of simulations versus best bandwidth in step 2 when selecting component values for the two-stage transimpedance amplifier.

TABLE IX
CHROMOSOME REPRESENTATION FOR COMPONENT SELECTION. THE TOP ROW SHOWS THE PARAMETER NAME FOR THE COMPONENT AND THE BOTTOM ROW SHOWS THE VALUE OF THAT PARAMETER

$W_1(\mu\text{m})$	$W_2(\mu\text{m})$	$W_3(\mu\text{m})$	$W_4(\mu\text{m})$	$W_5(\mu\text{m})$	$W_6(\mu\text{m})$	$R_F(\text{k}\Omega)$	$R_6(\text{k}\Omega)$
0.39	47.86	0.59	24.71	15.18	7.40	750.8	2798.8

2) *Component Selection for Fixed Architectures*: In this section, we use ASSENT to select component values for fixed architectures of two-stage and three-stage transimpedance amplifiers. Besides providing a comparison with the synthesis methodologies in [10], we also compare our results with an NN surrogate assisted GA.

Two-Stage Transimpedance Amplifier: We use ASSENT to determine the width of all the MOSFETs and resistors with the goal of minimizing the objective functions defined in Section VI-B1. We discretize the design space in step 1 by generating 100 Sobol samples for resistors in the $[100, 5\text{k}] \Omega$ range and width in the $[0.2, 50] \mu\text{m}$ range. These value ranges include those for the human-designed circuit. Table IX shows a chromosome for this case where W_i corresponds to the width of MOSFET T_i , and R_F and R_6 denote the resistors in Fig. 19.

We evolve a generation of 30 individuals for a maximum of 400 generations. We use a smaller population size than in architecture search because the problem is more straightforward due to a smaller design space. The stopping criteria are as follows: 1) the scaled bandwidth with respect to the human design falls below 1; 2) the number of generations exceeds 100 and bandwidth stays the same for more than 100 generations, indicating saturation; and 3) the maximum number of generations, i.e., 400, is reached.

Table X shows a comparison of the design synthesized by ASSENT with the designs obtained by other synthesis methodologies. The row named GA + NN surrogate uses an NN as a surrogate function within GA to provide a comparison with other metamodel-based optimization techniques like in [33] but with some modifications. We use GA instead of artificial bee colony optimization to handle output constraints. We train

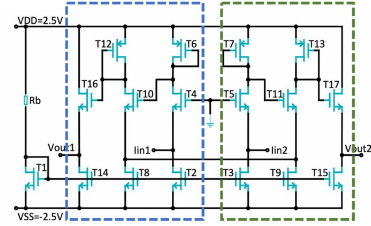


Fig. 23. Schematic of a three-stage differential transimpedance amplifier [10].

an NN after every generation on all valid simulations. We select an NN with one of the following architectures: $[(15), (30), (40, 20, 8)]$. We experimented with the same NN architecture choices as the ones used in step 2, but obtained a lower value of the objective function. We modify Algorithm 1 and generate $10\times$ candidate solutions in a generation using crossover and mutations. We select the best $P = 30$ candidate solutions after evaluating each using the surrogate NN. We report the solution that satisfies all the hard constraints and has the best value of the objective function.

The second last row of Table X shows the value of the objective function obtained after step 1. The bandwidth is inferior to that obtained in human design. Hence, in step 2, we fine-tune step 1 design through component selection to improve its performance. The last row of Table X shows the design synthesized using ASSENT. ASSENT is more than $6\times$ sample-efficient than DDPG and achieves the highest bandwidth among all considered designs. Fig. 22 plots the best bandwidth value versus the number of simulations used in step 2.

Three-Stage Transimpedance Amplifier: We select the component values for the three-stage transimpedance amplifier shown in Fig. 23, which is adapted from [10]. The blue and green dotted boxes contain subcircuits that are mirror images of each other. Hence, we obtain the component values for only one subcircuit and mirror them in the other. We determine the width and length of all the MOSFETs, including the bias transistor T1. There are 19 components in all: width/length of nine MOSFETs and a resistor R_b .

TABLE X
COMPARISON OF ASSENT DESIGNS WITH THOSE IN [10] FOR THE TWO-STAGE TRANSIMPEDANCE AMPLIFIER
(HARD CONSTRAINT VIOLATION SHOWN ENCIRCLED)

Spec	#Samples	Time	Noise (pA/ $\sqrt{\text{Hz}}$)	Gain (dB Ω)	Peaking (dB)	Power (mW)	Gate area (μm^2)	Bandwidth (GHz)
Human Design [10]	1,289,618	months	≤ 19.3	≥ 57.6	≤ 1	≤ 18	-	maximize
DDPG [10]	50,000	30 GPU hrs	18.6	57.7	0.927	8.11	23.11	5.95
Bayesian Opt. [10]	880	30 hrs	19.2	58.1	0.963	3.18	-	5.78
GA+NN surrogate	11,923	12.7 hrs	19.6	58.6	0.629	4.24	-	5.16
ASSENT Step 1	5,214	0.7 hr	18.0	57.7	0.863	6.73	23.27	5.72
ASSENT (Step 1+2)	7,853	77 hrs	19.2	58.5	0.645	5.51	17.86	5.71
				57.6	0.949	5.60	18.15	6.12

TABLE XI
COMPARISON OF DESIGNS SYNTHESIZED USING ASSENT WITH THOSE SYNTHESIZED IN [10] FOR THE THREE-STAGE TRANSIMPEDANCE AMPLIFIER (HARD CONSTRAINT VIOLATIONS SHOWN ENCIRCLED)

Spec	#Samples	Time	Bandwidth (MHz)	Gain (k Ω)	Power (mW)	Gate area (μm^2)
Human Design [10]	10,000,000	months	≥ 90	≥ 20	≤ 3	-
DDPG [10]	40,000	40 GPU hrs	90.1	20.2	1.37	211.0
Bayesian Opt. [10]	1,160	40 hrs	92.5	20.7	2.50	90.0
GA+NN surrogate	12,000	12.3 hrs	72.5	21.1	4.25	130.0
ASSENT Step 1	3,060	0.5 hr	91.7	25.7	2.93	246.6
ASSENT (Step 1+2)	5,749	84.7 hrs	90.2	22.9	4.96	337.0
			90.5	20.1	3.00	69.2

The objective is to minimize the sum of the gate areas of all the MOSFETs while meeting hard constraints for *gain*, *bandwidth*, and *power*. We discretize the design space during component selection in step 1 by generating 100 Sobol samples with width in the $[2, 30] \mu\text{m}$, length in the $[1, 2.2] \mu\text{m}$, and resistor in the $[50\text{k}, 500\text{k}] \Omega$ range. The human-synthesized circuit has a width in the $[2, 44] \mu\text{m}$ range, length in the $[1, 2] \mu\text{m}$ range, and a resistor of 291 k Ω . We reduce the design space for width by around 30% to encourage step 1 to obtain designs with a smaller area. We also round the length to the nearest 0.2 units since the technology only permits the length to be an integer multiple of 0.2 μm . We use this rounding in step 2 as well.

We have the following objectives.

- 1) *Bandwidth*: We set the passband to 90 MHz with a target gain of 35.57 k Ω (this corresponds to a gain of 85 dB for the half-circuit whereas the minimum gain required for its valid design is 80 dB or 20 k Ω differential gain). We use the following rewards/penalties.
 - a) A reward for a MOSFET operating in the saturation region, else a penalty is applied. We use a reward of 1 for operation in the saturation region. We apply a penalty of 5 (7) for operation in the linear (cutoff) region. Since the number of MOSFETs is larger than in the earlier design, we slightly increase these numbers to encourage MOSFET operation in the saturation region.
 - b) Penalty of 15 based on fractional deviation in gain below 80 dB (20 k Ω) for the half circuit in Fig. 23.
 - c) Penalty of 15 based on fractional deviation in bandwidth below 90 MHz.
- 2) *Area*: We define the area objective as the ratio of the sum of the areas of the MOSFET in one of the mirrored regions and the area of the bias MOSFET (T1) and the corresponding sum of areas in the human-synthesized circuit.
- 3) *Power*: We define this objective as the ratio between measured power and the power consumed by the

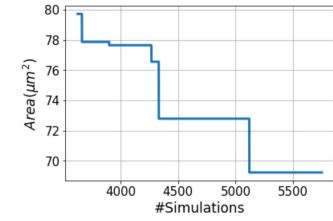


Fig. 24. Best area versus the number of simulations in step 2 when selecting component values for the three-stage transimpedance amplifier. Results are shown when the area drops below 80 μm^2 .

human-designed circuit, which is 1.37 mW. We levy a penalty of 15 based on the fractional deviation in power above this value.

We select an NN from the following architectures: $[(10), (50), (40, 20, 8)]$ when using GA + NN surrogate: same choices as the ones in step 2. The second last row of Table XI shows results of the circuit synthesized using step 1. This circuit violates the hard constraint on power and is hence not an acceptable design. The area of this circuit is also much higher than that of the human-designed circuit. Hence, in the next step, we fine-tune the component values to minimize the area while satisfying all the hard constraints. The last row of Table XI shows the results obtained by ASSENT. We set the initial requirement for the area to 80 μm^2 . ASSENT synthesizes a design that satisfies all the hard constraints with an area that is around 23% lower than the design obtained using DDPG. ASSENT is around 7 \times more sample-efficient than DDPG. Fig. 24 plots the best area value versus the number of simulations. The area is computed after rounding MOSFET length to the nearest 0.2 μm .

VII. CONCLUSION

In this article, we formulated nonlinear system design as an MOO problem and proposed a framework called ASSENT to solve it. We used gradient-free search through GA for exploration and CNMA for sample efficiency. CNMA achieves

sample efficiency by connecting NNs with MILP solvers in a new learning-from-failure feedback loop. The methodology provides a flexible framework for discovering efficient architectures and component values or simply the component values for a fixed architecture. Using this framework, we achieve the same or improve the value of the objective functions compared to designs synthesized using CNMA by up to 53%. We also synthesized electrical circuits with the best value of the objective function while improving sampling efficiency by 6–12×. As part of future work, we plan to formulate nonlinear system design as graph problems in order to explore different architectures by manipulating these graphs and other sample-efficient techniques for *active learning*. We also plan to enhance the efficacy of the methodology by combining it with RL.

ACKNOWLEDGMENT

The authors would like to thank Hanrui Wang for providing details of his work and the simulation environment used in [10]. The authors would also like to acknowledge the help provided by Sanjai Narain, Emily Mak, and Karthik Narayan with CNMA and various benchmarks used for the evaluation of ASSENT. The simulations presented in this article were performed on computational resources managed and supported by Princeton Research Computing at Princeton University. The views, opinions, and/or findings expressed are those of the authors and should not be interpreted as representing the official views or policies of the Department of Defense or the U.S. Government.

REFERENCES

- [1] K. Sampigethaya and R. Poovendran, "Aviation cyber-physical systems: Foundations for future aircraft and air transport," *Proc. IEEE*, vol. 101, no. 8, pp. 1834–1855, Aug. 2013.
- [2] A. O. Akmandor and N. K. Jha, "Keep the stress away with SoDA: Stress detection and alleviation system," *IEEE Trans. Multi-Scale Comput. Syst.*, vol. 3, no. 4, pp. 269–282, Oct./Dec. 2017.
- [3] Z. Zhou, Y. S. Ong, P. B. Nair, A. J. Keane, and K. Y. Lum, "Combining global and local surrogate models to accelerate evolutionary optimization," *IEEE Trans. Syst., Man, Cybern. C, Appl. Rev.*, vol. 37, no. 1, pp. 66–76, Jan. 2007.
- [4] S. Narain *et al.*, "Fast design space exploration of nonlinear systems: Part I," *IEEE Trans. Comput.-Aided Design Integr. Circuits Syst.*, early access, 2021.
- [5] G. Brockman *et al.* *OpenAI Gym*. (2016). [Online]. Available: <https://gym.openai.com>
- [6] E. Polak, D. Q. Mayne, and J. E. Higgins, "A superlinearly convergent algorithm for min-max problems," in *Proc. IEEE Conf. Decis. Control*, vol. 1, Tampa, FL, USA, 1989, pp. 894–898.
- [7] N. D. Kraus, "Wave glider dynamic modeling, parameter identification and simulation," Ph.D. dissertation, Dept. Mech. Eng., Univ. Hawaii at Manoa, Honolulu, HI, USA, May 2012.
- [8] Z. Wang, C. Gehring, P. Kohli, and S. Jegelka, "Batched large-scale Bayesian optimization in high-dimensional spaces," in *Proc. Int. Conf. Artif. Intell. Stat.*, 2018, pp. 745–754.
- [9] *OpenDSS, Electrical Power System Simulation Tool*. Accessed: Mar. 15, 2021. [Online]. Available: <https://smartgrid.epri.com/SimulationTool.aspx>
- [10] H. Wang, J. Yang, H.-S. Lee, and S. Han, "Learning to design circuits," 2018. [Online]. Available: [arXiv:1812.02734](https://arxiv.org/abs/1812.02734).
- [11] W. Lyu, F. Yang, C. Yan, D. Zhou, and X. Zeng, "Batch Bayesian optimization via multi-objective acquisition ensemble for automated analog circuit design," in *Proc. Int. Conf. Mach. Learn.*, 2018, pp. 3306–3314.
- [12] W. B. Powell, "A unified framework for stochastic optimization," *Eur. J. Oper. Res.*, vol. 275, no. 3, pp. 795–821, 2019.
- [13] V. Mnih *et al.*, "Playing Atari with deep reinforcement learning," in *Proc. NIPS Deep Learn. Workshop*, 2013.
- [14] T. P. Lillicrap *et al.*, "Continuous control with deep reinforcement learning," in *Proc. Int. Conf. Learn. Represent.*, 2016.
- [15] R. S. Zebulum, M. A. Pacheco, and M. M. B. Vellasco, *Evolutionary Electronics: Automatic Design of Electronic Circuits and Systems by Genetic Algorithms*. Boca Raton, FL, USA: CRC Press, 2018.
- [16] K. Deb, A. Pratap, S. Agarwal, and T. Meyarivan, "A fast and elitist multiobjective genetic algorithm: NSGA-II," *IEEE Trans. Evol. Comput.*, vol. 6, no. 2, pp. 182–197, Apr. 2002.
- [17] K. V. Price, *An Introduction to Differential Evolution, New Ideas in Optimization*. Maidenhead, U.K.: McGraw-Hill, 1999.
- [18] M. Dorigo, M. Birattari, and T. Stutzle, "Ant colony optimization," *IEEE Comput. Intell. Mag.*, vol. 1, no. 4, pp. 28–39, Nov. 2006.
- [19] J. Kennedy and R. Eberhart, "Particle swarm optimization," in *Proc. IEEE Int. Conf. Neural Netw.*, Perth, WA, Australia, 1995, pp. 1942–1948.
- [20] D. Zhou, J. Wang, B. Jiang, H. Guo, and Y. Li, "Multi-task multi-view learning based on cooperative multi-objective optimization," *IEEE Access*, vol. 6, pp. 19465–19477, 2018.
- [21] J. R. Koza, F. H. Bennett, D. Andre, M. A. Keane, and F. Dunlap, "Automated synthesis of analog electrical circuits by means of genetic programming," *IEEE Trans. Evol. Comput.*, vol. 1, no. 2, pp. 109–128, Jul. 1997.
- [22] J. D. Lohn and S. P. Colombano, "A circuit representation technique for automated circuit design," *IEEE Trans. Evol. Comput.*, vol. 3, no. 3, pp. 205–219, Sep. 1999.
- [23] G. Nicosia, S. Rinaudo, and E. Sciacca, "An evolutionary algorithm-based approach to robust analog circuit design using constrained multi-objective optimization," in *Proc. Int. Conf. Innovat. Techn. Appl. Artif. Intell.*, 2007, pp. 7–20.
- [24] A. Das and R. Vemuri, "GAPSYS: A GA-based tool for automated passive analog circuit synthesis," in *Proc. IEEE Int. Symp. Circuits Syst.*, Orleans, LA, USA, 2007, pp. 2702–2705.
- [25] K. Settaluri, A. Haj-Ali, Q. Huang, K. Hakhamaneshi, and B. Nikolic, "AutoCkt: Deep reinforcement learning of analog circuit designs," in *Proc. Design Autom. Test Eur. Conf. Exhibit.*, 2020, pp. 490–495.
- [26] A. Canelas *et al.*, "FUZY: A fuzzy c-means analog IC yield optimization using evolutionary-based algorithms," *IEEE Trans. Comput.-Aided Design Integr. Circuits Syst.*, vol. 39, no. 1, pp. 1–13, Jan. 2020.
- [27] R. A. de Lima Moreto, C. E. Thomaz, and S. P. Gimenez, "Gaussian fitness functions for optimizing analog CMOS integrated circuits," *IEEE Trans. Comput.-Aided Design Integr. Circuits Syst.*, vol. 36, no. 10, pp. 1620–1632, Oct. 2017.
- [28] R. Phelps, M. Krasnicki, R. A. Rutenbar, L. R. Carley, and J. R. Hellums, "Anaconda: Simulation-based synthesis of analog circuits via stochastic pattern search," *IEEE Trans. Comput.-Aided Design Integr. Circuits Syst.*, vol. 19, no. 6, pp. 703–717, Jun. 2000.
- [29] L. Vințan, R. Chiș, M. A. Ismail, and C. Coțofană, "Improving computing systems automatic multiobjective optimization through meta-optimization," *IEEE Trans. Comput.-Aided Design Integr. Circuits Syst.*, vol. 35, no. 7, pp. 1125–1129, Jul. 2016.
- [30] N. R. Dhanwada, A. Nunez-Aldana, and R. Vemuri, "A genetic approach to simultaneous parameter space exploration and constraint transformation in analog synthesis," in *Proc. IEEE Int. Symp. Circuits Syst. (ISCAS)*, vol. 6, Orlando, FL, USA, 1999, pp. 362–365.
- [31] G. Zheng, S. P. Mohanty, E. Kougianos, and O. Okobiah, "iVAMS: Intelligent metamodel-integrated Verilog-AMS for circuit-accurate system-level mixed-signal design exploration," in *Proc. IEEE Int. Conf. Appl. Spec. Syst. Archit. Process.*, Washington, DC, USA, 2013, pp. 75–78.
- [32] O. Garitselov, S. P. Mohanty, and E. Kougianos, "Fast optimization of nano-CMOS mixed-signal circuits through accurate metamodeling," in *Proc. Int. Symp. Qual. Electron. Design*, Santa Clara, CA, USA, 2011, pp. 1–6.
- [33] O. Garitselov, S. P. Mohanty, and E. Kougianos, "Fast-accurate non-polynomial metamodeling for Nano-CMOS PLL design optimization," in *Proc. Int. Conf. VLSI Design*, Hyderabad, India, 2012, pp. 316–321.
- [34] O. Garitselov, S. P. Mohanty, E. Kougianos, and O. Okobiah, "Metamodel-assisted ultra-fast memetic optimization of a PLL for WiMax and MMDS applications," in *Proc. Int. Symp. Qual. Electron. Design (ISQED)*, Santa Clara, CA, USA, 2012, pp. 580–585.
- [35] O. Okobiah, S. Mohanty, and E. Kougianos, "Fast design optimization through simple Kriging metamodeling: A sense amplifier case study," *IEEE Trans. Very Large Scale Integr. (VLSI) Syst.*, vol. 22, no. 4, pp. 932–937, Apr. 2014.

- [36] D. A. Van Veldhuizen and G. B. Lamont, "Evolutionary computation and convergence to a Pareto front," in *Proc. Late Breaking Papers Genet. Program. Conf.*, 1998, pp. 221–228.
- [37] D. E. Goldberg and J. H. Holland, *Genetic Algorithms and Machine Learning*. Boston, MA, USA: Kluwer Acad. Publ., 1988.
- [38] T. Blickle and L. Thiele, "A comparison of selection schemes used in evolutionary algorithms," *Evol. Comput.*, vol. 4, no. 4, pp. 361–394, Dec. 1996.
- [39] M. Akintunde, A. Lomuscio, L. Maganti, and E. Pirovano, "Reachability analysis for neural agent-environment systems," in *Proc. Int. Conf. Principles Knowl. Represent. Reas.*, 2018, pp. 1–10.
- [40] G. Venturini. *AhKab 0.18 Docs*. (2015). [Online]. Available: https://ahkab.readthedocs.io/en/latest/examples/Python_API.html
- [41] K. Deb and H. Jain, "An evolutionary many-objective optimization algorithm using reference-point-based nondominated sorting approach, part I: Solving problems with box constraints," *IEEE Trans. Evol. Comput.*, vol. 18, no. 4, pp. 577–601, Aug. 2014.
- [42] S. Burhenne, D. Jacob, and G. P. Henze, "Sampling based on Sobol sequences for Monte Carlo techniques applied to building simulations," in *Proc. Int. Conf. Build. Simulat.*, 2011, pp. 1816–1823.
- [43] Gurobi Optimization LLC. *Gurobi Optimizer Reference Manual*. (2020). [Online]. Available: <http://www.gurobi.com>
- [44] F. Chollet *et al.*. "Keras." [Online]. Available: <https://github.com/fchollet/keras> 2015.
- [45] F. Pedregosa *et al.*, "Scikit-learn: Machine learning in Python," *J. Mach. Learn. Res.*, vol. 12, pp. 2825–2830, Nov. 2011.
- [46] D. Izzo, "PyGMO and PyKEP: Open source tools for massively parallel optimization in astrodynamics (the case of interplanetary trajectory optimization)," in *5th Int. Conf. Astrodyn. Tools Techn. (ICATT)*, 2012. [Online]. Available: [http://www.esa.int/gsp/ACT/doc/MAD/pub/ACT-RPR-MAD-2012-\(ICATT\)PyKEP-PaGMO-SOCIS.pdf](http://www.esa.int/gsp/ACT/doc/MAD/pub/ACT-RPR-MAD-2012-(ICATT)PyKEP-PaGMO-SOCIS.pdf)
- [47] J. Duchi, E. Hazan, and Y. Singer, "Adaptive subgradient methods for online learning and stochastic optimization," *J. Mach. Learn. Res.*, vol. 12, no. 7, pp. 2121–2159, 2011.
- [48] H. Mao *et al.*, "Park: An open platform for learning-augmented computer systems," in *Proc. Neural Inf. Process. Syst.*, 2019, pp. 2494–2506.



Prerit Terway received the B.Tech. degree in electrical engineering from the Indian Institute of Technology Gandhinagar, Ahmedabad, India, in 2012, and the M.S. degree in electrical engineering from the University of Michigan at Ann Arbor, Ann Arbor, MI, USA, in 2014. He is currently pursuing the Ph.D. degree in electrical engineering with Princeton University, Princeton, NJ, USA.

His research interests include machine learning and cyber-physical systems.



Kenza Hamidouche received the bachelor's degree in computer science from the Ecole Nationale Supérieure d'Informatique, Oued Smar, Algeria, in 2012, the master's degree in computer science from the University of Rennes 1, Rennes, France, in 2013, and the Ph.D. degree in telecommunication from CentraleSupélec, Gif-sur-Yvette, France, in 2016.

In 2015, she was a Visiting Scholar with Virginia Tech, Blacksburg, VA, USA. She is currently a Postdoctoral Researcher with Princeton University, Princeton, NJ, USA. Her research interests are in

the broad areas of game theory, learning under uncertainty, and reinforcement learning. Applications of particular interest include wireless communications, Internet of Things, pricing, autonomous multiagent systems, security, and privacy.



Niraj K. Jha (Fellow, IEEE) received the B.Tech. degree in electronics and electrical communication engineering from the Indian Institute of Technology Kharagpur, Kharagpur, India, in 1981, and the Ph.D. degree in electrical engineering from the University of Illinois at Urbana-Champaign, Champaign, IL, USA, in 1985.

He has been a Faculty Member with the Department of Electrical Engineering, Princeton University, Princeton, NJ, USA, since 1987. He has coauthored five books that are widely used. His

research interests include smart healthcare, cybersecurity, machine learning, and monolithic 3-D IC design.

Dr. Jha has received the Princeton Graduate Mentoring Award. He has served as the Editor-in-Chief for IEEE TRANSACTIONS ON VERY LARGE SCALE INTEGRATION (VLSI) SYSTEMS and as an associate editor of several other journals. His research has won 20 best paper awards or nominations. He has given several keynote speeches in the areas of nanoelectronic design/test, smart healthcare, and cybersecurity. He was given the Distinguished Alumnus Award by IIT, Kharagpur. He is a Fellow of ACM.